RESEARCH ARTICLE | DECEMBER 11 2023

Non-alloyed ohmic contacts to (010) β -Ga₂O₃ with low contact resistance \bigcirc

Kathleen T. Smith \square \square ; Cameron A. Gorsak \square ; Avijit Kalra \square ; Bennett J. Cromer \square ; Kathy Azizie \square ; Daniel M. Dryden \square ; Darrell G. Schlom \square ; Debdeep Jena \square ; Hari P. Nair \square ; Huili Grace Xing \square

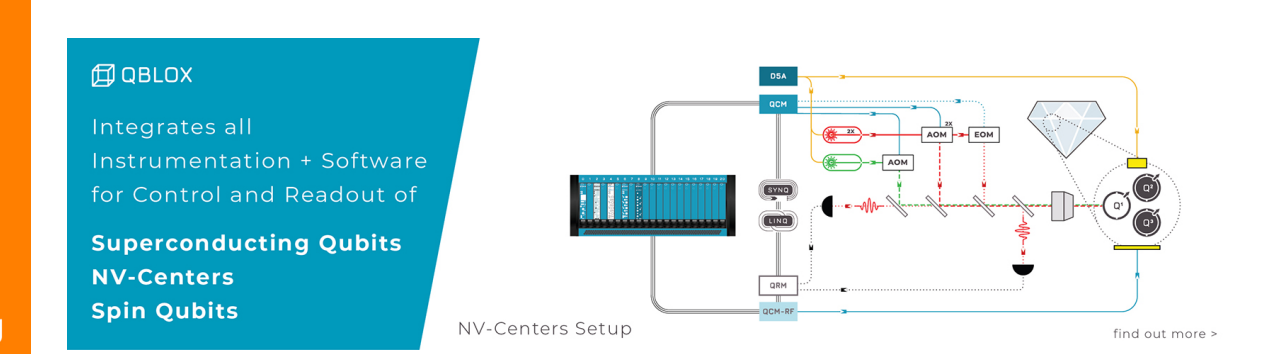


Appl. Phys. Lett. 123, 242101 (2023) https://doi.org/10.1063/5.0177618





CrossMark





Non-alloyed ohmic contacts to (010) β -Ga₂O₃ with low contact resistance

Cite as: Appl. Phys. Lett. **123**, 242101 (2023); doi: 10.1063/5.0177618 Submitted: 22 September 2023 · Accepted: 19 November 2023 · Published Online: 11 December 2023







Kathleen T. Smith,^{1,a)} © Cameron A. Gorsak,² © Avijit Kalra,³ © Bennett J. Cromer,² © Kathy Azizie,² © Daniel M. Dryden,⁴ © Darrell G. Schlom,^{2,5} © Debdeep Jena,^{2,5,6} © Hari P. Nair,² © and Huili Grace Xing^{2,5,6} ©

AFFILIATIONS

- ¹School of Applied and Engineering Physics, Cornell University, Ithaca, New York 14853, USA
- ²Department of Materials Science and Engineering, Cornell University, Ithaca, New York 14853, USA
- School of Chemical and Biomolecular Engineering, Cornell University, Ithaca, New York 14853, USA
- ⁴Air Force Research Laboratory, Sensors Directorate, Wright-Patterson AFB, Ohio 45433, USA
- ⁵Kavli Institute at Cornell for Nanoscale Physics, Cornell University, Ithaca, New York 14853, USA

ABSTRACT

Low resistance non-alloyed ohmic contacts are realized by a metal-first process on homoepitaxial, heavily n^+ doped (010) β -Ga₂O₃. The resulting contacts have a contact resistance (R_c) as low as 0.23 Ω -mm on an as-grown sample and exhibit nearly linear ohmic behavior even without a post-metallization anneal. The metal-first process was applied to form non-alloyed contacts on n^+ (010) β -Ga₂O₃ grown by metal-organic chemical vapor deposition (MOCVD) as well as suboxide molecular beam epitaxy. Identical contacts fabricated on similar MOCVD samples by conventional liftoff processing exhibit highly rectifying Schottky behavior. Re-processing using the metal-first process after removal of the poor contacts by conventional methods does not improve the contacts; however, addition of a Ga-flux polishing step followed by re-processing using a metal-first process again results in low resistance, nearly linear ohmic contacts. The liftoff process, therefore, does not reliably render nearly linear ohmic behavior in non-alloyed contacts. Furthermore, no interface contamination was detected by x-ray photoelectron spectroscopy. This suggests that during the initial liftoff processing, a detrimental layer may form at the interface, likely modification of the Ga₂O₃ surface, that is not removable during the contact removal process but that can be removed by Ga-flux polishing.

Published under an exclusive license by AIP Publishing. https://doi.org/10.1063/5.0177618

 β -Ga₂O₃ is an ultra-wide bandgap (4.5–4.9 eV) semiconductor that has emerged as a promising candidate for power and RF device applications due to its favorable material properties, including the availability of low-cost native substrates, wide range of demonstrated doping densities, electron mobility up to 200 cm²/V-s, and high critical electric field (E_c). Vertical and lateral transistors have been demonstrated with kV-breakdown, and lateral devices have achieved an average E_c surpassing the unipolar limits for GaN and SiC.^{2–4} The high E_c of Ga₂O₃ allows for aggressive source–drain scaling of devices in order to minimize on-state resistance at a given breakdown voltage. For such devices, contact resistance (R_c) becomes a significant contributor to the overall series resistance and, subsequently, to both on-state conduction losses and switching speed.

For high-speed applications above GHz, low R_c is required. Attaining low R_c on wide bandgap semiconductors is challenging due to Fermi level pinning and a lack of sufficiently low work function

metals, which prevents formation of a junction with no energy barrier to conduction. Instead, techniques that generate a tunnel junction by forming heavily doped regions underneath the contacts using Si-ion implantation, spin-on glass, and selective area regrowth of heavily doped material, coupled with alloyed contacts, are favored. $^{5-9}$ Ohmic contact formation on $\rm Ga_2O_3$ using Ti/Au has been attributed to the formation of a thin Ti–TiO $_x$ layer that acts as an intermediate semi-conductor layer. 10,11

Non-alloyed (i.e., as-deposited) contacts are a desired approach to better understand the energy band alignment, e.g., surface Fermi pinning near the conduction band edge, between a heavily doped semiconductor and a metal or another intermediate semiconductor such as TiO_x . Most reported ohmic contacts, however, are alloyed. Villora *et al.* reported non-alloyed linear contacts on bulk (010) substrates (n $\sim 10^{17} - 10^{18} \, \text{cm}^{-3}$) by sputtering Ti/Al; no R_c was extracted due to the substrate thickness. ¹² Higashiwaki *et al.* reported Ti/Au

⁶School of Electrical and Computer Engineering, Cornell University, Ithaca, New York 14853, USA

a) Author to whom correspondence should be addressed: kts57@cornell.edu

ohmic contacts on bulk (010) Sn-doped substrates (n \sim 5 \times 10¹⁷ cm⁻³) only after removing the top layer by reactive ion etch (RIE). Again, no R_c was extracted due to the thick substrate. Zhou *et al.* reported Ti/Al/Au on the (100) orientation using β -Ga₂O₃ flakes (n \sim 8 \times 10¹⁸ cm⁻³) after an Ar plasma pretreatment, resulting in R_c of 1.7 Ω -mm. On the (010) surface, Alema *et al.* reported contacts to $1-3\times10^{20}$ cm⁻³ doped (010) β -Ga₂O₃ with specific contact resistance (ρ_c) as low as 1.12×10^{-6} Ω cm², but ρ_c still improved by an order of magnitude after alloying, even at a reported donor concentration as high as 3×10^{20} cm⁻³. Since 2.5×10^{-10} cm⁻³.

Furthermore, ohmic contact processing, typically performed using a liftoff process, has historically given inconsistent results in non-alloyed contacts. Figure 1(a) shows I–V curves from non-alloyed TLM patterns across four nominally similar, heavily doped ($N_d > 5 \times 10^{19}~{\rm cm}^{-3}$) metal organic chemical vapor deposition (MOCVD)-grown samples. The current not only varies by approximately 12 orders of magnitude between different samples but even by approximately six orders of magnitude across the same sample.

In this work, we demonstrate non-alloyed, nearly linear ohmic contacts using a metal-first process on heavily doped (010) β-Ga₂O₃ grown by MOCVD. In a metal-first process, a blanket metal layer is deposited, and then photoresist is used to pattern the metal with wet or dry etching. Thus, the Ga₂O₃ surface is not exposed to photoresist prior to metal/Ga₂O₃ contact formation. This contrasts with the conventional liftoff process where photoresist is deposited and patterned prior to metal deposition. Furthermore, we repeat the metal-first process on material grown by other methods and show that the resulting contacts are more consistent both within and between samples than contacts fabricated by liftoff [Fig. 1(b)]. Moreover, we investigate contacts formed by a liftoff process on similar material and discover that, after removal of faulty contacts, ohmic contacts cannot be formed even by subsequent metal-first processing. However, following Ga-flux polishing of the surface, non-alloyed ohmic contacts are formed using the metal-first process. 16,17 We attribute the initial barrier to conduction to the formation of an interfacial layer during the liftoff process, and the

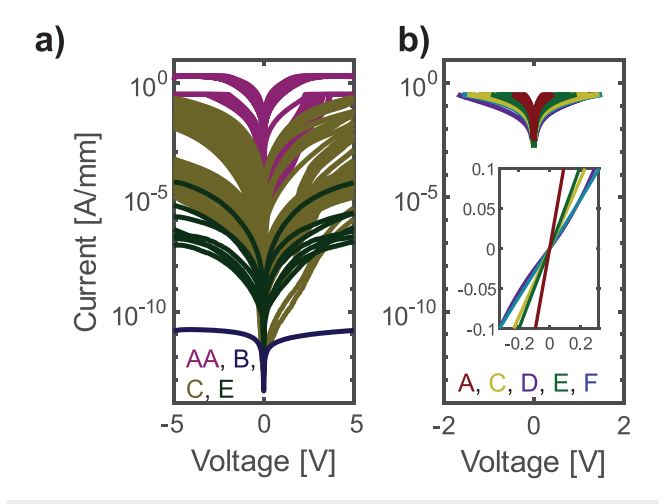


FIG. 1. I–V curves from non-alloyed Ti/Au contacts formed by (a) a conventional lift-off process vs (b) a metal-first process. Curves from the same sample are the same color. Contact performance is far more consistent both within and between samples for the metal-first process.

subsequent improvement to the removal of that layer during Ga-flux polishing. This is consistent with plasma-etch assisted formation of non-alloyed ohmic contacts. 12,13 X-ray photoelectron spectroscopy (XPS) of the contact interfaces of both ohmic and non-conductive contacts reveals the expected spontaneous formation of a Ti–TiO_x layer near the Ga_2O_3 interface, but it does not identify any foreign contaminants. This is consistent with earlier transmission electron microscopy studies, where a chemically clean interface is observed between the as-deposited Ti and Ga_2O_3 , but the liftoff contacts are not ohmic. 18

The *in situ* doped samples (A–C) were grown in an Agnitron Agilis 100 MOCVD system on an Fe-doped (010) β -Ga₂O₃ substrate. Before loading into the reactor, samples were dipped in a 48% HF bath for 30 min to reduce the interfacial Si.¹⁹ For sample A, a 50 nm unintentionally doped (UID) layer followed by a 250 nm heavily doped layer was grown. Growth details for all MOCVD samples may be found in the supplementary material. The sample was then diced in half and solvent cleaned. Hall measurements on a previously grown calibration sample give a channel charge, mobility, and sheet resistance (R_{sh}) of 7×10^{19} cm⁻³, 89.2 cm²/V-s, and 39.9 Ω / \Box , respectively.

Figure 2 provides diagrams of the process modules used across the various samples. Sample A was solvent cleaned, then Ti/Au (10/110 nm) was deposited by electron-beam evaporation in a load-locked Angstrom evaporator at a base pressure of 1×10^{-8} Torr. Circular transfer length method (CTLM) patterns were defined using contact photolithography. The metal stack was then wet etched in TFA Gold Etchant for 45 s followed by 90 s in 30:1 BOE. Figure 2(d) shows the metal-first process.

For samples B and C, a 102.5 nm UID layer followed by a 160 nm doped layer was grown, then diced in half and solvent cleaned. Hall measurements on an immediately prior grown calibration sample give a channel charge, mobility, and R_{sh} of 9.8×10^{19} cm⁻³, 79.5 cm²/V-s, and 52.3 Ω/\Box , respectively. Unlike for sample A, samples B and C were initially patterned with both linear and circular TLM patterns and, therefore, required mesa isolation to prevent current spreading in the linear structures. Mesa isolation was performed by inductively coupled plasma (ICP)-RIE etching using BCl₃/Ar chemistry with a Ti/Ni hard mask. TLM patterns were defined by contact lithography. Then, an ohmic Ti/Au (50/110 nm) stack was deposited by electron-beam evaporation in a CVC SC4500 bell jar evaporator at a base pressure of 1.3×10^{-6} Torr and lifted off. Figure 2(a) shows the liftoff process. The TLM patterns were measured and then the contacts were removed by 5 min in 1:1 HF:HNO₃ and 30 s in TFA Gold Etchant. The samples were then treated with ozone for 9 min, followed by a 5 min 49% HF

Sample B was then immediately loaded into the vacuum chamber of the load-locked evaporator (5 min estimated air exposure) and underwent the same metal-first process as sample A. Sample C was loaded into a Veeco Gen 930 molecular beam epitaxy (MBE) system (30 min estimated air exposure), with a base pressure of 5×10^{-9} Torr. Using a Knudsen cell as the Ga source, Ga-flux polishing was performed for 4 min with a Ga flux of 1.4×10^{-7} Torr and a substrate temperature of $850\,^{\circ}$ C as measured by a beam flux monitor and thermocouple at the substrate. The etch rate for these conditions is approximately $2.5\,$ nm/min. Figures 2(b) and 2(c) show the contact strip and Ga-flux polish modules. The sample was then unloaded from the MBE (15 min estimated air exposure) and soaked in 37% HCl for $15\,$ min to remove the backside indium mounting. Sample C was immediately loaded into the SC4500 electron-beam evaporator and

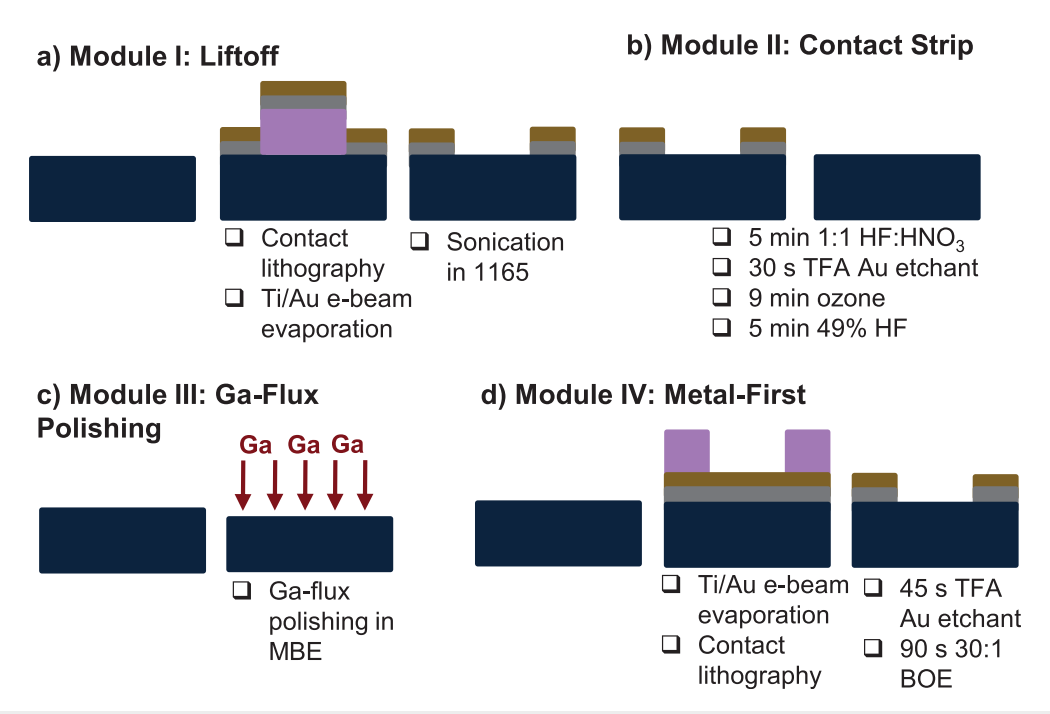


FIG. 2. Diagrams of the (a) liftoff, (b) contact strip, (c) Ga-flux polishing, and (d) metal-first process modules.

50/110 nm Ti/Au was deposited at a base pressure of 2×10^{-6} Torr and patterned using the wet-etch described earlier.

To confirm the repeatability of these results across material grown by multiple methods, sample D, a 1 μ m thick *in situ* Si-doped β -Ga₂O₃ sample on Fe-doped (010) β -Ga₂O₃ substrate, was grown by suboxide MBE (S-MBE) in a Veeco Gen10 MBE system. Growth details are available in the supplementary material. Sample D has a carrier concentration of 3.0×10^{19} cm⁻³, confirmed by secondary ion mass spectroscopy, and a mobility of 62 cm²/V-s via Hall measurements. Sample D was processed using an identical metal-first process to sample A. Table I provides a summary of all samples reported in this work. Fabrication details for samples AA, E, and F may be found in the supplementary material.

The CTLM patterns were measured using a Keithley 4200 semiconductor characterization system in a four-point probe configuration using the correction factor outlined by Krämer.²¹ A Thermo Nexsa G2 XPS with Al-Kα source was used to correlate contact performance and chemical composition. The CTLM patterns have an inner radius of 50 μm and a pad spacing of 3–12 \pm 0.2 μm , confirmed by scanning electron microscopy. Figure 3(a) shows the I–V curves from a CTLM pattern with 5 μm pad spacing on samples A–C. Measurements on samples B and C are shown both after liftoff processing and after the contact strip and metal-first reprocessing, with sample C having a Gaflux polish between the liftoff and metal-first processes. While sample A shows nearly linear ohmic behavior, sample B is nonconductive for both the liftoff and metal-first process, and sample C pre-Ga-flux polishing shows highly rectifying Schottky behavior. After Ga-flux polishing and metal-first re-processing, however, sample C shows nearly linear ohmic behavior similar to sample A.

For sample A, the extracted R_{sh} from the CTLM is 41 Ω/\Box , which matches the Hall data from the calibration sample [Fig. 3(b)]. A non-alloyed R_c of 0.23 Ω -mm and ρ_c of 1.3 \times 10⁻⁵ Ω -cm² were recorded at a current bias of 50 mA. This contact resistance is competitive with reported contacts to (010) β -Ga₂O₃. Over the entire

TABLE I. Summary of sample information and processing.

Sample	Growth method	Doping (cm ⁻³)	Thickness (nm)	$R_{sh}\left(\Omega/\Box\right)$	Process modules	Non-alloyed R_c (Ω -mm)
AA	MOCVD	9×10^{19}	200	44	I	
A	MOCVD	7×10^{19}	250	40	IV	0.23
В	MOCVD	1×10^{20}	160	50	I, II, IV	
C	MOCVD	1×10^{20}	160	50	I, II, III, IV	0.73
D	S-MBE	3×10^{19}	1000	34	IV	0.81
E	MOCVD	5×10^{19}	220	76	I, II, III, IV	0.46
F	MOCVD	8×10^{19}	70	73	IV	0.41

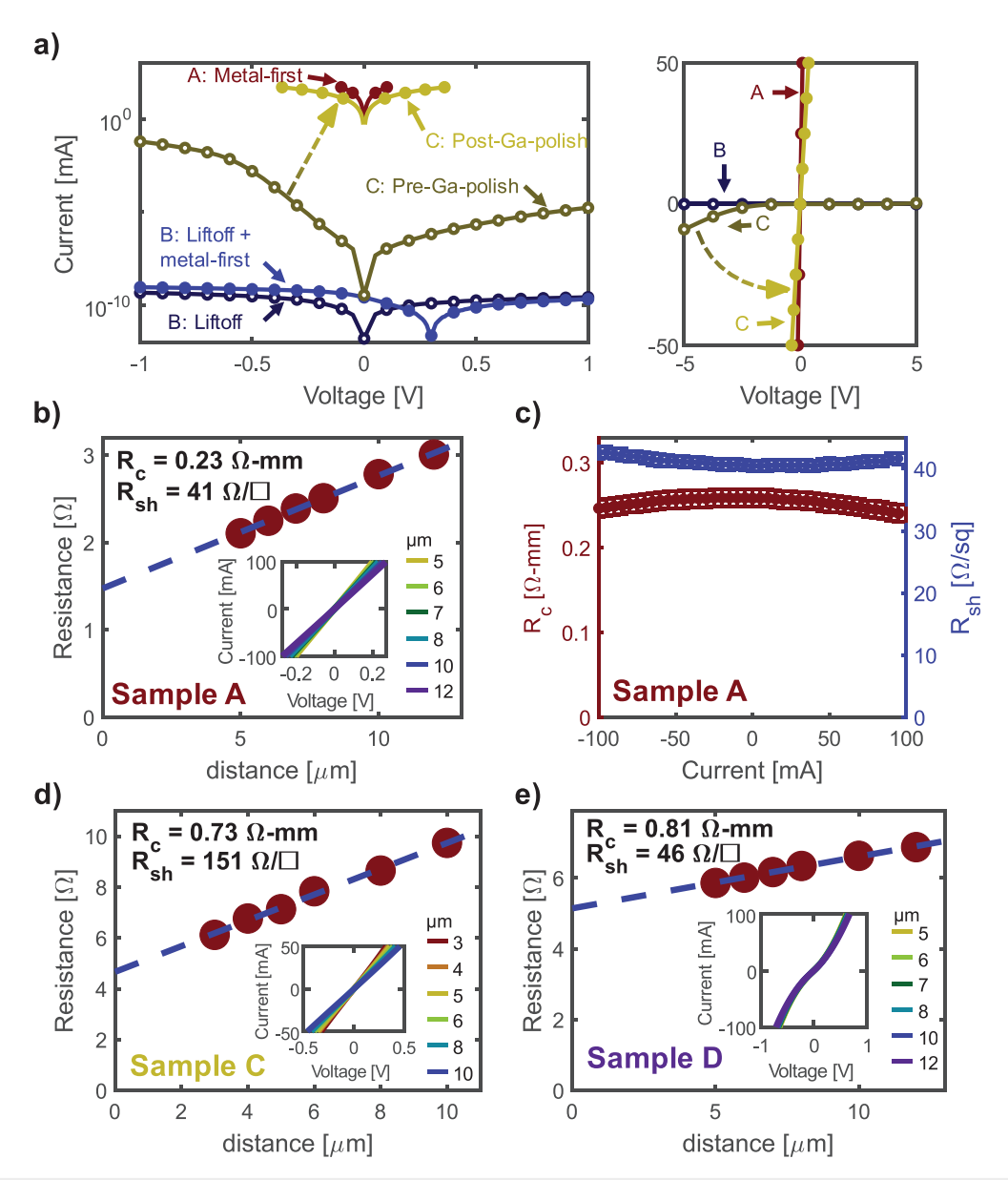


FIG. 3. (a) I–V curves for sample A (red), sample B (blue), and sample C (yellow). Data obtained from the liftoff process is indicated with open symbols, with filled symbols for the metal-first process. While both samples B and C were re-processed using a metal-first process, only sample C received Ga-flux polishing. (b) TLM measurements for metal-first processing on sample A (as grown by MOCVD) give 0.23 Ω -mm. (c) Average R_c and R_{sh} values for five CTLM patterns on sample A are shown over the full 100 mA applied current range. TLM measurements for (d) metal-first processing of sample C post Ga-flux polish and (e) metal-first processing on sample D (as grown by S-MBE) give 0.73 and 0.81 Ω -mm, respectively, at 50 mA applied bias.

100 mA measurement range, the contact behavior is nearly linear ohmic [Fig. 3(c)]. Sample F, discussed in full in the supplementary material, provides comparable results.

TLM extraction of R_c and R_{sh} is not possible for sample B and sample C prior to Ga-flux polishing. For sample C post Ga-flux polishing, however, a non-alloyed R_c of 0.73 Ω -mm and ρ_c of 3.4 \times 10⁻⁵ Ω -cm² are extracted from the CTLM at an applied current bias of 50 mA [Fig. 3(d)]. The extracted R_{sh} 151 Ω/\square , is three times higher

than the original Hall data. Future studies should aim to investigate the effects of each of these processes independently on contact formation. Sample E, discussed in full in the supplementary material, was also Ga-flux polished and re-processed with a thinner Ti layer and yields similar results to sample C.

For sample D, the resulting contacts are slightly leaky Schottky and CTLM measurements yield an R_{sh} of 46 Ω/\Box , R_c of 0.81 Ω -mm, and ρ_c of $1.4 \times 10^{-4} \Omega$ -cm² at 50 mA applied current [Fig. 3(e)].

The higher contact resistance and less ideal behavior is attributed to the lower doping level in the sample, which results in a thicker tunneling barrier to charge conduction.

Sample AA is the only contact fabricated by liftoff for which R_c is reported in this work. The sample is discussed in full in the supplementary material. Despite the very high doping level (9 \times 10 19 cm $^{-3}$), as-deposited contacts were Schottky-like and no R_c could be extracted. After alloying, the contacts were linear ohmic with an R_c of 0.19 Ω -mm. The observation that select liftoff-processed contacts can be made linear-ohmic by alloying, whereas metal-first contacts on similar material, or even at lower doping levels, are ohmic as-deposited further indicates adverse effects of the liftoff process that are circumvented by a metal-first process.

The apparent recovery of the surface of sample C following Ga-flux polishing is attributed to the removal of an interface layer that was formed during initial liftoff processing. This same interfacial layer is presumed to be the reason that re-processed contacts using the metal-first contact process on sample B were not ohmic. However, the depth-resolved XPS profiles of non-alloyed contacts on samples A and B show very similar atomic profiles [Figs. 4(a) and 4(b)]. The overlap of the gold, titanium, and gallium signals despite a lack of alloying are attributed partially to the finite escape depth of photo-electrons (\sim 0.5–5 nm, depending on material and binding energy). The measurement, therefore, is sensitive to a few nanometers at the surface of the sample, rather than the single monolayer composition of the sample surface. The overlap is also partially attributable to non-uniform

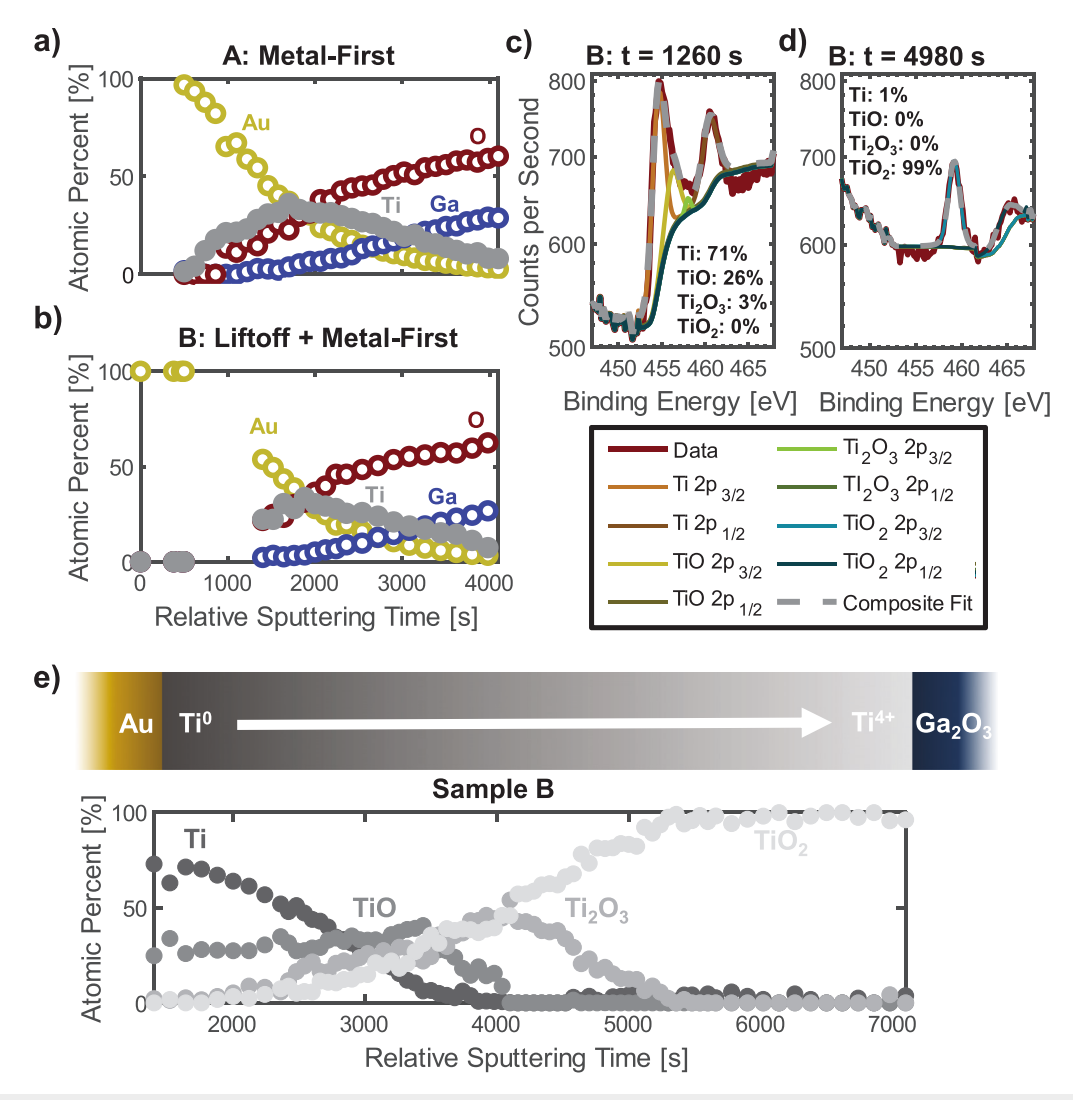


FIG. 4. Depth-resolved elemental composition of (a) sample A (as-grown metal-first process) and (b) sample B (liftoff followed by metal-first without Ga-flux polishing). Only Au, Ti, Ga, and O signatures are detected, besides adventitious carbon contamination on the Au surface prior to sputtering (not shown). Chemical bonding analysis of the Ti2_p peak for sample B near (c) the Au/Ti interface and (d) the $\text{Ti/Ga}_2\text{O}_3$ interface reveals a shift in oxidation state from Ti^0 near the Au interface to Ti^{4+} near the Ga_2O_3 interface. (e) The oxidation state of Ti in sample B plotted over the entire Ti layer shows that the Ti layer is fully oxidized to Ti^{4+} for approximately 2–3 nm near the Ga_2O_3 interface, assuming a reasonably constant sputtering rate during depth profiling.

sputtering due to sample charging, and the gold tail especially may be further attributed to sputtered material redeposition of softer materials. As has been reported previously, even for non-alloyed contacts, spontaneous formation of a few nanometer Ti-TiOx layer at the Ga2O3 interface at room temperature is observed.²² Analysis of the chemical bonding state based on the shift in binding energy of the Ti2, peak for sample B shows that the composition of the titanium layer shifts from mostly Ti^0 near the Au/Ti interface [Fig. 4(c)] to entirely Ti^{4+} near the Ti/Ga₂O₃ interface [Fig. 4(d)]. This transition is observed both for ohmic and non-conductive contacts. The full depth profile of the titanium layer [Fig. 4(e)] for sample B further shows that the entire titanium layer (10 nm as-deposited) is at least partially oxidized and suggests that 2-3 nm at the Ga₂O₃ interface are fully oxidized to Ti⁴⁺. Since the partially oxidized Ti ($TiO_x > 50\%$ at. %) thickness is about 8 nm, it also suggests that 10-nm Ti is sufficient to provide nonalloyed ohmic contacts to Ga₂O₃; however, the effects of the Ti thickness in alloyed ohmic contacts most likely need to be reevaluated given the insights of this study.

As for the source of the poor contact performance, the depthprofile of sample B does not indicate any contaminants at the interface. Any foreign contaminants from the liftoff process, e.g., photoresist residue, are therefore below the detection limit (0.1-1 at. %) of the XPS system. It is surprising to see that the modification of the Ga₂O₃ surface during liftoff is so significant that a high tunneling barrier is created such that resultant contacts are highly Schottky-like even on n+ Ga₂O₃ doped with Si, a shallow dopant, at a concentration as high as 1×10^{20} cm⁻³. In comparison, similar non-alloyed contacts on n⁺ GaN doped with Si at a concentration > 10¹⁹ cm⁻³, which has a similar charge neutrality level and dopant activation energy, are readily linear and ohmic. In this study, we chose to use Ga-flux polishing to minimize the influence of plasma damage on the Ga2O3, which is widely known yet poorly understood and controlled, as non-alloyed linear contacts using plasma treatment have been attained but with very high resultant R_c. ²³ It is also worth noting that the nonlinear nonalloyed contacts to n⁺ Ga₂O₃ in this study (e.g., sample B and sample C pre-Ga-polish) typically exhibit linear I–V behavior upon annealing, similar to reports in the literature; however, they have a wide array of R_c values (not shown). Further investigation of the Ga₂O₃ surface following various steps of the liftoff process is merited to identify the potential source of the poor interface.

In conclusion, we report non-alloyed Ti/Au contacts on n⁺ homoepitaxial (010) β -Ga₂O₃ with R_c as low as 0.23 Ω -mm (corresponding to a ρ_c of $1.3 \times 10^{-5} \ \Omega$ -cm²) on an as-grown sample using a metal-first process. Figure 5 benchmarks reported ohmic contact resistance in Ω -mm (most relevant in lateral devices) as a function of the doping concentration directly underneath the contact. This benchmark exercise reveals that the non-alloyed metal-first contacts are competitive with the current state of the art, especially when compared to contacts with commensurate doping concentration. Furthermore, we attain non-alloyed metal-first contacts on material grown by S-MBE in addition to MOCVD, demonstrating the versatility of this process across sample growth methods. In addition, we demonstrate improved repeatability and consistency of contact performance both across individual samples and between similar samples with the metal-first process compared to conventional liftoff processing. Finally, we demonstrate Ga-flux polishing as a viable technique to recover the quality of the Ga₂O₃ surface after unsuccessful ohmic

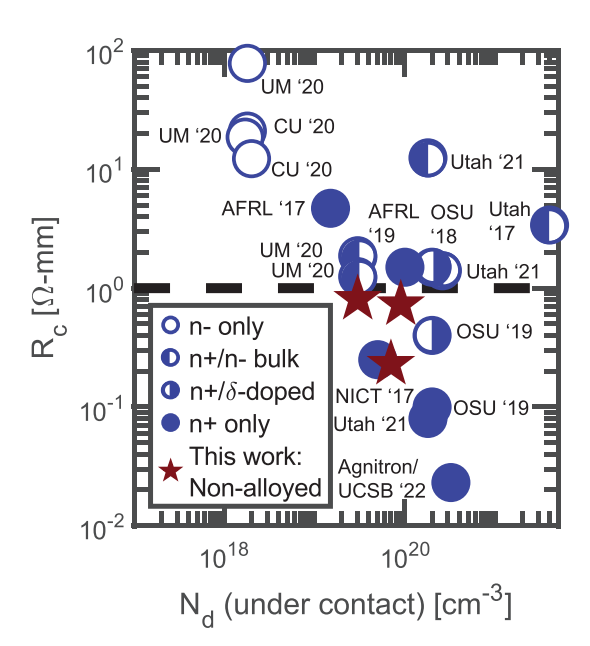


FIG. 5. Benchmarking of ohmic contacts on (010) β -Ga₂O₃ with respect to the doping level underneath the contact. The non-alloyed metal-first contacts are highly competitive, especially with contacts to materials of commensurate n^+ doping concentration. ^{6,8,9,15,24–30}

contact processing via liftoff. The contact formation techniques reported here are hoped to assist in reliable fabrication of low-resistance ohmic contacts for high-speed device performance.

See the supplementary material for additional sample growth and fabrication details, as well as discussions of the TLM measurements for samples AA, E, and F, which are largely beyond the scope of this work.

This work was in part supported by ACCESS, an AFOSR Center of Excellence (No. FA9550-18-1-0529). This work was supported in part by SUPREME, one of the seven centers in JUMP 2.0, a Semiconductor Research Corporation (SRC) program sponsored by DARPA. The device fabrication was performed in part at the Cornell Nanoscale Facility, a NNCI member supported by NSF Grant No. NNCI-2025233. This work used facilities and instrumentation supported by the NSF through the Cornell University Materials Research Science and Engineering Center DMR-1719875. We thank Jon Wright at Cornell CCMR for many fruitful discussions on XPS technique and analysis.

AUTHOR DECLARATIONS Conflict of Interest

The authors have no conflicts to disclose.

Author Contributions

Kathleen Tyrie Smith: Conceptualization (equal); Data curation (equal); Formal analysis (equal); Investigation (lead); Methodology (equal); Visualization (equal); Writing – original draft (lead). **Huili Grace Xing:** Conceptualization (equal); Data curation (equal); Formal

analysis (equal); Funding acquisition (lead); Methodology (equal); Resources (equal); Supervision (equal); Visualization (equal); Writing – review & editing (equal). Cameron A. Gorsak: Investigation (supporting); Resources (lead); Writing – review & editing (equal). Avijit Kalra: Investigation (supporting). Bennett Cromer: Formal analysis (supporting); Investigation (supporting). Kathy Azizie: Resources (supporting); Writing – review & editing (supporting). Daniel M. Dryden: Formal analysis (supporting); Writing – review & editing (equal). Darrell G. Schlom: Funding acquisition (supporting); Supervision (supporting). Hari P. Nair: Funding acquisition (supporting); Supervision (supporting).

DATA AVAILABILITY

The data that support the findings of this study are available from the corresponding author upon reasonable request.

REFERENCES

- ¹A. J. Green, J. Speck, G. Xing, P. Moens, F. Allerstam, K. Gumaelius, T. Neyer, A. Arias-Purdue, V. Mehrota, A. Kuramata, K. Sasaki, S. Watanabe, K. Koshi, J. Blevins, O. Bierwagen, S. Krishnamoorthy, K. Leedy, A. R. Arehart, A. T. Neal, S. Mou, S. A. Ringel, A. Kumar, A. Sharma, K. Ghosh, U. Singisetti, W. Li, K. Chabak, K. Liddy, A. Islam, S. Rajan, S. Graham, S. Choi, Z. Cheng, and M. Higashiwaki, APL Mater. 10, 029201 (2022).
- ²W. Li, K. Nomoto, T. Nakamura, D. Jena, and H. G. Xing, in *IEEE International Electron Devices Meeting (IEDM)* (IEEE, 2019), pp. 12.1.4–12.4.4.
 ³S. Sharma, K. Zeng, S. Saha, and U. Singisetti, IEEE Electron Device Lett. 41, 836 (2020).
- ⁴A. J. Green, K. D. Chabak, E. R. Heller, R. C. Fitch, M. Baldini, A. Fiedler, K. Irmscher, G. Wagner, Z. Galazka, S. E. Tetlak, A. Crespo, K. Leedy, and G. H. Jessen, IEEE Electron Device Lett. 37, 902 (2016).
- ⁵K. Sasaki, M. Higashiwaki, A. Kuramata, T. Masui, and S. Yamakoshi, Appl. Phys. Express 6, 086502 (2013).
- ⁶K. Zeng, J. S. Wallace, C. Heimburger, K. Sasaki, A. Kuramata, T. Masui, J. A. Gardella, and U. Singisetti, IEEE Electron Device Lett. **38**, 513 (2017).
- ⁷K. D. Leedy, K. D. Chabak, V. Vasilyev, D. C. Look, J. J. Boeckl, J. L. Brown, S. E. Tetlak, A. J. Green, N. A. Moser, A. Crespo, D. B. Thomson, R. C. Fitch, J. P. McCandless, and G. H. Jessen, Appl. Phys. Lett. 111, 012103 (2017).

- ⁸Z. Xia, H. Xue, C. Joishi, J. McGlone, N. K. Kalarickal, S. H. Sohei, M. Brenner, A. Arehart, S. Ringel, S. Lodha, W. Lu, and S. Rajan, IEEE Electron Device Lett. 40, 1052 (2019).
- ⁹A. Bhattacharyya, S. Roy, P. Ranga, D. Shoemaker, Y. Song, J. S. Lundh, S. Choi, and S. Krishnamoorthy, Appl. Phys. Express 14, 076502 (2021).
- ¹⁰M. H. Lee and R. L. Peterson, APL Mater. 7, 022524 (2019).
- ¹¹M. H. Lee and R. L. Peterson, J. Mater. Res. **36**, 4771 (2021).
- ¹²E. G. Villora, K. Shinamura, T. Ujiie, and K. Aoki, Appl. Phys. Lett. **92**, 202118 (2008).
- ¹³M. Higashiwaki, K. Sasaki, A. Kuramata, T. Masui, and S. Yamakoshi, Appl. Phys. Lett. 100, 013504 (2012).
- ¹⁴H. Zhou, K. Maize, G. Qiu, A. Shakouri, and P. D. Ye, Appl. Phys. Lett. 111, 092102 (2017).
- ¹⁵F. Alema, C. Peterson, A. Bhattacharyya, S. Roy, S. Krishnamoorthy, and A. Osinsky, IEEE Electron Device Lett. 43, 1649 (2022).
- ¹⁶M.-Y. Tsai, O. Bierwagen, M. E. White, and J. S. Speck, J. Vac. Sci. Technol., A 28, 354–359 (2010).
- ¹⁷N. K. Kalarickal, A. Fielder, S. Dhara, H.-L. Huang, A. F. M. A. U. Bhuiyan, M. W. Rahman, T. Kim, Z. Xia, Z. J. Eddine, A. Dheenan, M. Brenner, H. Zhao, J. Hwang, and S. Rajan, Appl. Phys. Lett. 119, 123503 (2021).
- ¹⁸M. H. Lee and R. L. Peterson, ACS Appl. Mater. Interfaces 12, 46277 (2020).
- ¹⁹A. Bhattacharyya, C. Peterson, T. Itoh, S. Roy, J. Cooke, S. Rebolloa, P. Ranga, B. Sensale-Rodriguez, and S. Krishnamoorthy, APL Mater. 11, 021110 (2023).
- A. Kalra, M.S. thesis, Cornell University, 2023.
- ²¹M. C. J. C. M. Krämer, M.S. thesis, Technical University of Eindhoven, 2000.
- ²²M. H. Lee and R. L. Peterson, J. Solid State Sci. Technol. 8, Q3176 (2019).
- ²³W. Li, D. Saraswat, Y. Long, K. Nomoto, D. Jena, and H. G. Xing, Appl. Phys. Lett. **116**, 192101 (2020).
- ²⁴K. Chabak, A. Green, N. Moser, S. Tetlak, J. McCandless, K. Leedy, R. Fitch, A. Crespo, and G. Jessen, in IEEE Device Research Conference (DRC), 2017.
- ²⁵M. H. Wong, Y. Nakata, A. Kuramata, S. Yamakoshi, and M. Higashiwaki, Appl. Phys. Express 10, 041101 (2017).
- ²⁶Z. Xia, C. Joishi, S. Krishnamoorthy, S. Bajaj, Y. Zhang, M. Brenner, S. Lodha, and S. Rajan, IEEE Electron Device Lett. 39, 568 (2018).
- ²⁷K. J. Liddy, A. J. Green, N. S. Hendricks, E. R. Heller, N. A. Moser, K. D. Leedy, A. Popp, M. T. Lindquist, S. E. Tetlak, G. Wagner, K. D. Chabak, and G. H. Jessen, Appl. Phys. Express 12, 126501 (2019).
- ²⁸K. Smith, E. Long, W. Li, K. Nomoto, D. Jena, and H. G. Xing, in Semiconductor Interface Specialists Conference (SISC), 2020.
- ²⁹E. Long, M.S. thesis, Cornell University, 2021.
- ³⁰A. Bhattacharyya, P. Ranga, S. Roy, C. Peterson, F. Alema, G. Seryogin, A. Osinsky, and S. Krishnamoorthy, IEEE Electron Device Lett. 42, 1272 (2021)